Interpreting the Carbon Isotope Record of Mass Extinctions

Martin Schobben[1], Bas van de Schootbrugge[1], and Paul B. Wignall[2]

1811-5209/19/0015-0331$2.50 DOI: 10.2138/gselements.15.5.331

Mass extinctions are global-scale environmental crises marked by the loss of numerous species from all habitats. They often coincide with rapid changes in the stable carbon isotope ratios ($^{13}C/^{12}C$) recorded in sedimentary carbonate and organic matter, ratios which can indicate substantial inputs to the surface carbon reservoirs and/or changes in the cycling of carbon. Models to explain these changes have provided much fuel for debate on the causes and consequences of mass extinctions. For example, the escape of methane from gas hydrate deposits or the emission of huge volumes of gaseous carbon from large-scale volcanic systems, known as large igneous provinces, may have been responsible for decreases of $^{13}C/^{12}C$ in sedimentary deposits. In this article, we discuss the challenges in distinguishing between these, and other, alternatives.

KEYWORDS: carbon cycle, large igneous provinces, greenhouse gas, climate, Earth system feedback

MASS EXTINCTIONS

The fossil record reveals that the evolution of life has been punctuated by several catastrophic events that eliminated species globally (Raup and Sepkoski 1982). After the Cambrian Period (~500 million years ago), five mass extinction events have been identified (colloquially known as "the big five"), but there have been numerous smaller extinction events. Most of these crises coincided with voluminous flood basalt eruptions associated with so-called large igneous provinces (LIPs) (Wignall 2015; Black and Gibson 2019 this issue). Only one, the famous event at the end of the Cretaceous, has been confidently linked to a giant bolide impact (Alvarez et al. 1980). However, not all episodes of giant LIP volcanism coincided with extinction events: for example, major episodes of flood basalt eruption during the Early Cretaceous and the early Paleogene occurred during very low rates of extinction (FIGS. 1 AND 2) (Wignall 2015). Factors such as the composition of the upper crust through which the LIPs are intruded and whether the basalts were emplaced as subaerial or submarine lavas might explain some of the differences. But the eruption style is not readily correlated with the severity of any biotic disturbance (Svensen et al. 2009; Burgess et al. 2017; Johansson et al. 2018). The role of LIPs in global extinctions is, therefore, enigmatic, but clues to the link between the deep mantle and the biosphere come from perturbations of the biogeochemical carbon cycle as revealed by the sedimentary carbon record and, especially, the changing ratios of constituent stable carbon isotopes. There are many proposed links between LIPs, mass extinctions, and carbon cycle changes, including cooling and acid rain (by SO_2 degassing and aerosol formation), greenhouse warming (by CO_2 and CH_4 degassing), heavy metal pollution, and ozone layer depletion. There are also more intricate scenarios that involve plant die-off, enhanced soil erosion, and elevated weathering, which, in turn, increases the amount of nutrients reaching the oceans and so causes eutrophication, dissolved-oxygen depletion ("marine anoxia"), and turbidity. Many of these changes could have had an impact on the sedimentary carbon isotope record, and it is our challenge to distinguish the different impacts from the different causes on the carbon isotope record.

UNDERSTANDING THE CARBON CYCLE WITH CARBON ISOTOPE GEOCHEMISTRY

The isotopes of carbon have the same number of protons but differ in the number of neutrons, and so the mass of the atoms differs. The exact carbon isotope composition of a substance will depend on both kinetic and equilibrium effects (see the introduction of this issue of *Elements* for further details on carbon isotopes). As a reference, stable carbon isotope ratios are, by convention, denoted relative to the Vienna Peedee Belemnite (VPDB). We generally express deviations from this reference value, or when comparing different substances, as "lower" or "higher" (lower means the sample has less ^{13}C than the standard, or the natural, isotope abundance). But we can also refer to the product in a chemical reaction as being "enriched" (or "depleted") in ^{13}C (or ^{12}C). The carbon isotope values are expressed using the delta (δ) notation in "parts per thousand" (‰), and is derived by the following equation:

$$\delta^{13}C = \left(\frac{(^{13}C/^{12}C)_{sample} - (^{13}C/^{12}C)_{reference}}{(^{13}C/^{12}C)_{reference}} \right) \times 1{,}000$$

The process, known as isotope fractionation, causes a relative partitioning of the stable isotopes among substances and thereby changes their isotope composition. This is seen in the different pools of carbon on the Earth's surface. For example, the dissolved inorganic carbon (DIC) in the ocean has higher $\delta^{13}C$ values than the organic carbon of plankton in the ocean. The production

1 Department of Earth Sciences Utrecht University
Princetonlaan 8A
3584 CB Utrecht, The Netherlands
E-mail: m.a.n.schobben@uu.nl; b.vanderschootbrugge@uu.nl

2 School of Earth and Environment
University of Leeds
Leeds, LS2 9JT, UK
E-mail: P.B.Wignall@leeds.ac.uk

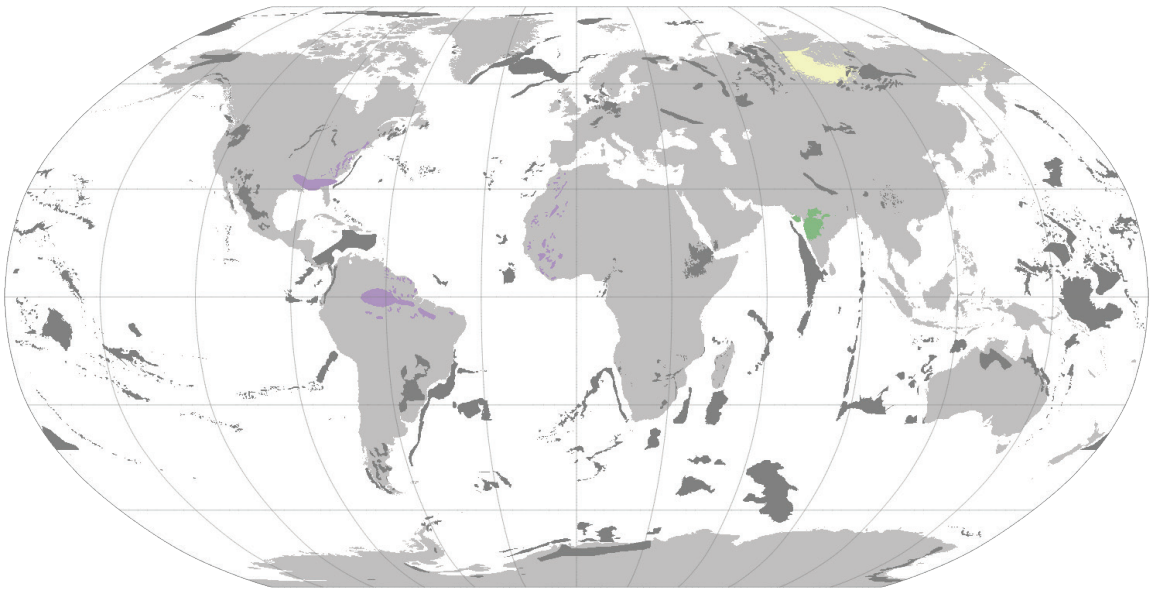

Figure 1 Geographic map of flood basalt deposits. Color codes are as follows: Siberian Traps (Russia) = yellow; Central Atlantic Magmatic Province (CAMP) = violet; Deccan Traps (India) = green; other large igneous provinces = dark grey. Land = light grey. Data from Johansson et al. (2018); reconstruction with GPlates (www.gplates.org).

of organic matter during photosynthesis is an enzyme-mediated process, which is accompanied by a large carbon isotope fractionation that preferentially selects the light ^{12}C isotope and shifts the material's $\delta^{13}C$ to 25‰ lower values on average. In contrast, carbon isotope partitioning during carbonate mineral precipitation causes only a small fractionation ($\delta^{13}C$ values are higher by 1‰–2‰ at Earth's surface temperatures, based on experimental results) and, therefore, closely approximate the DIC values of the contemporary ocean. These fluxes remove carbon from the ocean–atmosphere system and are balanced, on geological timescales (>100 ky), by carbonate alkalinity (CO_3^{2-} and HCO_3^-), carbon input through continental weathering, and CO_2 and CH_4 release by metamorphism and via volcanic outgassing. The combined effect of all these fluxes dictates the size and isotope composition of Earth's surface carbon reservoirs (Fig. 3). On geological timescales, the oceanic DIC pool and atmospheric CO_2 behave as one reservoir, because of the continuous exchange between them. This system is known as the long-term biogeochemical carbon cycle, where subtle imbalances in the volcanic and metamorphic carbon input, and the combination of weathering and organic carbon burial, modulate atmospheric CO_2 levels and, thus, climate over time. These subtle changes are recorded in the carbonate and organic matter in sedimentary rocks and allow us to study the history of this cycle using $\delta^{13}C$ records. Table 1 lists some of the frequently used carbon isotope recording mediums.

CARBON ISOTOPE CHANGES DURING MASS EXTINCTIONS

The stratigraphic carbon isotope record is generally stable, but this situation is often different during major extinction intervals when high amplitude (up to 8‰) positive or negative carbon isotope excursions (CIEs) occur. These changes are interpreted as evidence for major perturbations of the long-term biogeochemical carbon cycle, and they provide significant clues as to the nature of ancient crises. These carbon cycle perturbations are thought to be responsible for the rapid and significant climate changes that themselves can cause severe habitat degradation and mass extinction. Here, we focus on the carbon isotope record of the last three mass extinction events (Fig. 2): the Permian–Triassic, the Triassic–Jurassic, and the Cretaceous–Paleogene extinctions. We will first evaluate which sedimentary record(s) (Table 1) most faithfully reflect the functioning of the carbon cycle during these ancient

Table 1 Isotope recording mediums, respective carbon reservoirs recorded by the medium, and the advantages and disadvantages of each medium.

Isotope recording medium	Carbon reservoir	Advantage	Disadvantage
Bulk organic carbon	Dissolved inorganic carbon and atmospheric CO_2	Easy to sample.	Unspecific; mixture of different tissues and organisms with widely diverging physiologies.
n-alkanes*	Atmospheric CO_2	Specific biomarker of land plant leaf waxes.	Elaborate analytical process. Can be affected by biotic effects.
Bulk carbonate carbon	Dissolved inorganic carbon	Easy to sample.	Mixtures of carbonate precipitated at different water depths, carbonate minerals/polymorphs and produced by a range of organisms. Affected by diagenesis to a certain degree.
Foraminifera shells	Dissolved inorganic carbon	Better screening for diagenesis. Specific for a single species of organism living at a certain water depth.	Can be affected by biotic effects.

* long-chained *n*-alkanes with a predominant odd-over-even chain length are biomarkers assigned to land plant leaf waxes.

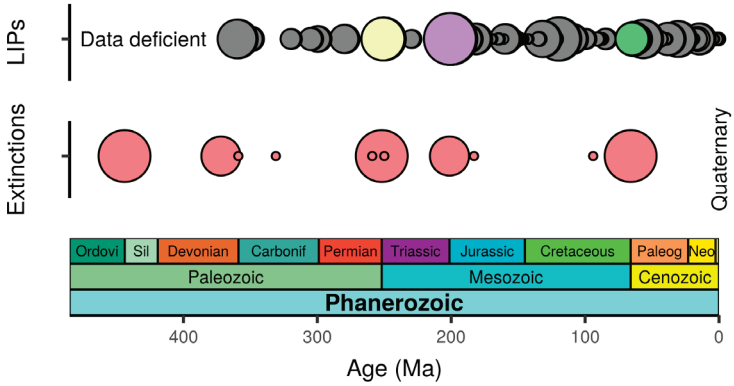

Figure 2 Temporal distribution of large igneous provinces (LIPs) and mass extinctions since the Ordovician. Color codes for LIPs are that in Figure 1. The size of LIP dots corresponds to LIP eruption size, from small (<< 0.1 Mkm^2) to large (1.8 Mkm^2). The size of the orange extinction dots correspond to extinction severity: small (3rd order, meaning generic diversity loss of less than 20%), medium (2nd order, meaning generic diversity loss of between 20% and 35%) and large (1st order, generic diversity loss of more than 35%). LIP data from Johansson et al. (2018) and paleontological data from various sources.

crises. In the following section, we will try to deconvolve those records in terms of cause and consequence, list the mechanism(s) that are most acceptable in the context of current understanding of the respective mass extinction event, and discuss the biological consequences of the proposed mechanisms.

A complicating factor, when comparing $\delta^{13}C$ records from different extinction events, is the variable nature of the sample sources available (Table 1). For example, the widespread occurrence of Permian-to-Triassic limestones from the Tethys realm (which formed in the shelf seas of the vast Tethys Ocean) has provided many carbonate-derived $\delta^{13}C$ records for the Permian–Triassic (P–Tr) mass extinction. These $\delta^{13}C$ records are obtained from bulk rock samples, which warrants caution because biogenic carbonates consist of clasts, matrix, and secondary calcite precipitates. These components can have different isotopic values, and so variations in their proportions can alter the $\delta^{13}C$ value even when there is no change in the ocean signal. This choice is, however, often unavoidable during mass extinctions due to the elimination of many calcifying organisms (Knoll et al. 2007). Notwithstanding, $\delta^{13}C$ records from different regions in the world often show similar trends, such as seen in P–Tr boundary sediments which show the same, uniform, >100 ky trend of a 4‰–5‰ lowering of $\delta^{13}C$ (e.g., in Iran, the Italian Alps, South China, Tibet, Oman, and Hungary) (Fig. 4). Transient (<100 ky) negative CIEs superimposed on the first-order trend have also been recognized at this time (Cao et al. 2009). However, increased scatter around the mean first-order trend in the post-extinction rock record (Fig. 4) might reflect a shift to a non-skeletal (microbial) carbonate production in the extinction's aftermath. In addition, the scatter has probably increased due to the incorporation of spatially diverse diagenetic signals produced in unborrowed anoxic sediments (Schobben et al. 2017). As a result of the low signal-to-noise ratio in bulk rock $\delta^{13}C$ records, the global significance of these secondary CIEs is hard to demonstrate. As an alternative, bulk organic matter from the P–Tr rock record has been used for carbon isotope analysis. However, these organic matter–based $\delta^{13}C$ records are not always able to reproduce the trend in carbonate-based $\delta^{13}C$ records, and ^{13}C-enriched bulk organics might reflect a turnover in the primary producers from eukaryotic- to prokaryotic-dominated plankton communities (Cao et al. 2009). While bulk organic matter–based $\delta^{13}C$ records can represent an environmental and/or ecological meaningful signal, they are not necessarily related to the long-term carbon cycle. This effect is, above all, controlled by the whole-rock organic material, which is a mixture of organic compounds that can differ in carbon isotopic signature by >10‰ (van de Schootbrugge et al. 2008).

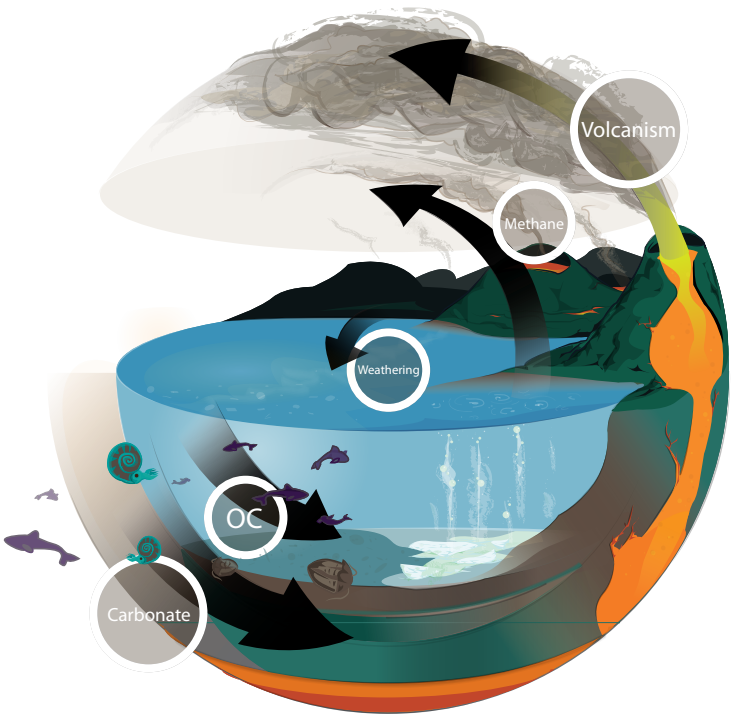

Figure 3 The biogeochemical carbon cycle. Note that the methane here derives from ocean-bottom methane clathrates (light green) Abbreviation: OC = organic carbon. Credit: Mark Schobben.

While lithological successions spanning the Triassic–Jurassic (Tr–J) mass extinction are generally devoid of carbonate, carbon isotope records from this time have mostly been derived from bulk organic matter. This is despite the fact that, like the P–Tr carbonate carbon isotope record, some continuous carbonate-bearing successions are available from the Tethyan and Panthalassian regions. However, the direct correlation of carbonate-based stratigraphic $\delta^{13}C$ records with those measured on organic matter is still largely unclear (van de Schootbrugge et al. 2008). Accepting the limitations of bulk organic matter–based $\delta^{13}C$ records, then an apparently variable stratigraphic $\delta^{13}C$ signal could simply reflect varying mixtures of organic compounds with different isotopic values. One solution to this problem is to meticulously separate the bulk organic matter into its individual constituents; another is to produce compound-specific $\delta^{13}C$ records. Thus, by screening the organic matter content of the Tr–J boundary section at Kuhjoch (Austria), Ruhl et al. (2010) showed that carbon isotope fluctuations were largely (but not completely) independent of organic matter compositional changes. One of the most outstanding features of the Tr–J record is an initial, negative CIE of up to 6‰–8‰, seen in many sections, developed over a brief timespan (<100 ky), and recorded in both whole-rock and compound-specific organic material (Ruhl et al. 2010, 2011) (Fig. 5). As the signal is also seen in organic molecules assigned to plant leaf waxes (long-chained *n*-alkanes with a predominant odd-over-even chain length), it could indicate that the carbon isotope signal records a change in atmospheric CO_2 (Ruhl et al. 2011). However, *n*-alkane extracts can also

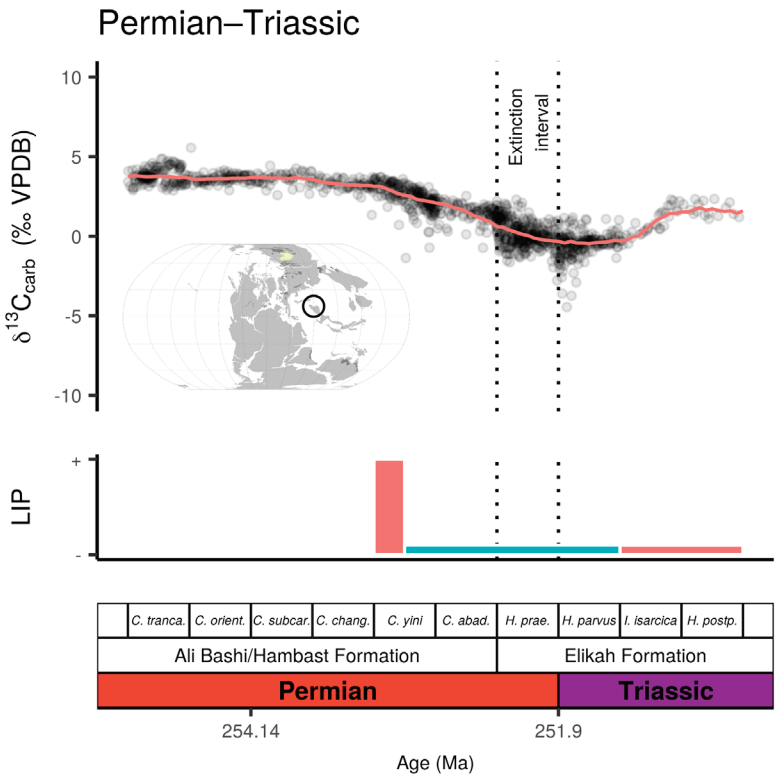

Figure 4 (**upper graph**) Composite carbon isotope curve for the Permian–Triassic boundary interval based on carbonate rock exposed in Iran (black circle on paleogeographic map, itself color coded as per Figure 1). The samples come from the Elikah Formation and both the Alibashi Formation and the Hambast Formation. Data from Schobben et al. (2017). Trendline and conodont biozonation scheme follows Schobben et al. (2017). Conodont biozones, from oldest to youngest, are shown in the top row of the table at the bottom of the image (abbreviations: C = *Clarkina*, H = *Hindeodus*, I = *Isarcicella*). Abbreviation: VPDB = Vienna Peedee belemnite. (**lower graph**) The relative intensity of large igneous provinces (LIPs) are correlated with the upper graph: red = extrusive phases; blue = intrusive phases. After Burgess et al. (2017).

be sourced from different plants with potentially species-specific carbon isotope values (van de Schootbrugge et al. 2008 and references therein). A floral turnover could, therefore, have been skewed to plant communities with a particularly ^{13}C-depleted signature in their leaf waxes. Moreover, changes in water availability can affect physiological processes and these could be expressed as differences in the magnitudes of carbon isotope fractionations, thereby potentially changing the δ^{13}C of the leaf waxes of a single plant species over time.

Notwithstanding the limitations discussed above, compound-specific organic carbon isotope analyses currently represent the most faithful record of a carbon cycle perturbation at the Tr–J boundary interval. The initial negative CIE is followed by heavier values and then a long-term trend of up to 4‰ lower δ^{13}C recorded in bulk organic matter (the so-called main CIE) (Fig. 5). However, independent confirmation of this second negative CIE of the Tr–J δ^{13}C record is still largely missing. In this respect, it is important to note that Tr–J sections located in Europe (and also other sites around the world) are marked by pronounced sedimentological, mineralogical, and paleontological changes over this interval, changes that have been associated with sea-level fluctuations, local extinctions of fauna and flora, and/or modulations of the continental weathering flux (von Hillebrandt et al. 2013). These observations warrant caution when interpreting the main CIE, because organic matter compositional changes could have biased this record (van de Schootbrugge et al. 2008). It therefore would seem that compound-specific δ^{13}C records over broader stratigraphic ranges across the Tr–J boundary interval would be a particularly high-priority target for future studies.

For the Cretaceous–Paleogene (K–Pg) mass extinction, the δ^{13}C changes across this interval are primarily obtained from the carbonate shells of foraminifera. This is in contrast to, for example, the P–Tr event, where it is not possible to construct such high-resolution single-component δ^{13}C records. Foraminifera shells only became major constituents of open marine sediments after the Tr–J extinction event. Foraminifera shells provides many benefits for geochemists. Modern foraminifera precipitate carbonate shells in close equilibrium with marine DIC and are assumed to provide a record of oceanic changes in K–Pg times. In addition, manual selection of individual specimens of foraminifera from sediments allows for screening to eliminate diagenetic alteration, such as recrystallization and crystal overgrowths. Usefully, foraminifera also inhabit both seafloor (benthic) and water column (planktic) settings, allowing the reconstruction of water column gradients of δ^{13}C values. Nonetheless, it is important to bear in mind that species-specific physiological aspects (e.g., growth rate and photosymbionts) and environmental parameters (e.g., CO_3^{2-} concentrations) also influence foraminiferal carbonate δ^{13}C.

The K–Pg crisis differs from the previous two mass extinctions in that there is either no, or only a moderate, 0.5‰–1‰ trend to lower or higher δ^{13}C across the event horizon (Zachos et al. 1989; D'Hondt et al. 1998). Prior to the extinction, planktic foraminifera show δ^{13}C values that are up to 2‰ more enriched with ^{13}C than contemporaneous benthic foraminifera (Fig. 6). This difference disappears at the K–Pg boundary and the two values converge before gradually separating again over the next 300 ky.

WHAT DO CARBON ISOTOPE CHANGES TELL US ABOUT MASS EXTINCTIONS?

A plethora of hypotheses have been proposed to explain the P–Tr CIE. Here are three popular ones: 1) a sudden overturn of a stagnant ocean that caused ^{13}C-depleted deep waters to merge into surface waters where the Tethyan limestones formed (Knoll et al. 1996); 2) a sea-level lowering and exposure of shelf sediments, which then weather to release ^{13}C-depleted carbon from their stored organic content (Holser and Magaritz 1987); 3) a collapse of primary productivity that caused ^{13}C-depleted carbon to return to the DIC pool and be incorporated into limestones (Rampino and Caldeira 2005). All of these mechanisms fail to correspond with either geological or modelling evidence. The first hypothesis actually contradicts the oceanic changes observed at the P–Tr boundary, because this event is marked by a replacement of relatively well-ventilated oceans by anoxic oceans (Hotinski et al. 2001) and it is unlikely that such an overturn would produce a >100 ky first-order δ^{13}C trend (Fig. 4). The second does not accord with current evidence of P–Tr sea-level change,

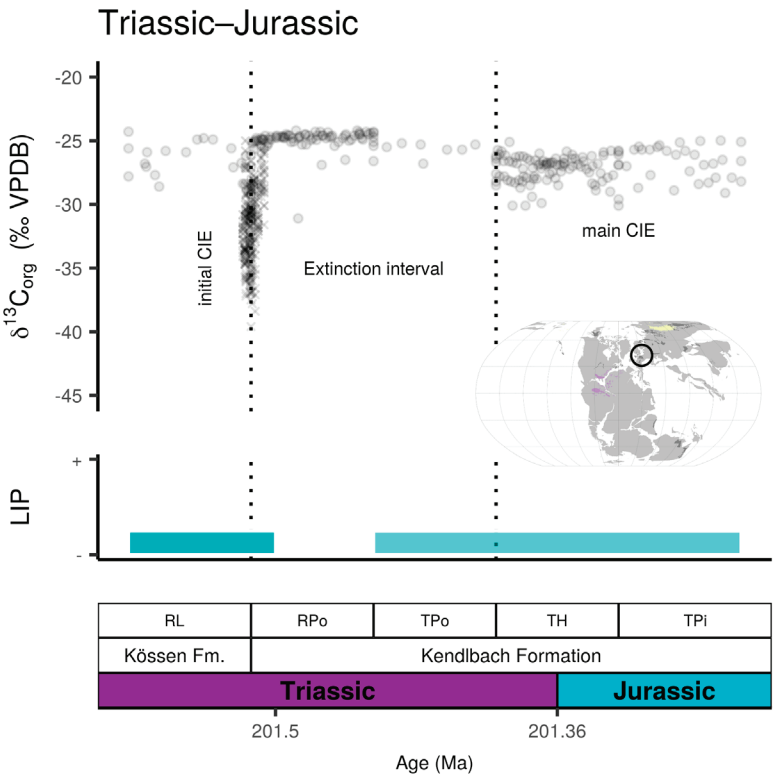

Figure 5 (**upper graph**) Carbon isotope curve for the Triassic–Jurassic boundary interval of the Northern Calcareous Alps (Austria; black circle on paleogeographic map, which itself is color coded as per Figure 1), using data from the Kössen Formation ["Fm" on figure] and the Kendlbach Formation, where the medium is either bulk organic matter (dots) or long-chained *n*-alkanes (crosses). Data from von Hillebrandt et al. (2013) and Ruhl et al. (2011). Palynostratigraphical zonation, from oldest to youngest is as follows: RL = *Rhaetipollis–Limbosporites* Assemblage Zone; RPo = *Ricciisporites–Polypodiisporites* Assemblage Zone; TPo = *Trachysporites–Porcellispora* Assemblage Zone; TH = *Trachysporites–Heliosporites* Assemblage Zone; TPi = *Trachysporites–Pinuspollenites* Assemblage Zone. After von Hillebrandt et al. (2013). Abbreviations: CIE = carbon isotope excursion; VPDB = Vienna Peedee belemnite. (**lower graph**) LIP intensity demarcates intrusive phases of CAMP (Central Atlantic Magmatic Province). After Heimdal et al. (2018).

which recognizes a short-term regression followed by a major transgression (Hallam and Wignall 1999). Finally, the third hypothesis is unlikely because multiple lines of evidence suggest that persisting (or increased) primary productivity and consequent oxygen demand is necessary to drive the spread of anoxic water masses during the extinction interval (Meyer et al. 2008).

The LIP Siberian Traps basalts are implicated in the P–Tr extinction and contemporaneous carbon cycle perturbations, and many scenarios have been developed based on this link. Unfortunately, the carbon isotope record is considered to be a poor monitor of eruptions because volcanic carbon emissions have been assumed to have a carbon isotope value of ~–5‰, which is only slightly lighter than the value in the oceans to which it is being added (3‰–4‰ for the Late Permian). If one accepts this assumption, then even giant eruptions are only capable of causing minor alterations to the prevailing DIC $\delta^{13}C$ values. For the specific example of the Siberian Traps, improved dating of the lava flows suggest that volcanic carbon release may not have been especially important in the extinction process because up to two-thirds of the Siberian Traps lavas may have been erupted before the extinction (Burgess et al. 2017) (Fig. 4). Instead, the main carbon release could have been caused by sill emplacement in the sedimentary basins beneath these flood basalts. This second volcanic phase does overlap in time with the extinction horizon (Fig. 4). Such intrusions would have baked the country rocks, which included both evaporites and organic-rich strata, and caused the escape of large volumes of halocarbons and very ^{13}C-depleted (down to –50‰) methane and carbon dioxide (thermogenic gases). Evidence for this process comes from the presence of numerous breccia pipes in the region, which are interpreted to be the product of explosive gas-release events (Svensen et al. 2009). Thus, the P–Tr CIE is now often attributed to both direct (volcanogenic) and indirect (thermogenic) gas emissions from the Siberian Traps, with the latter probably having the greatest influence on the decrease of $\delta^{13}C$ values. The consequent effects of thermogenic gas release are potentially more catastrophic, including ozone damage by halocarbons and global warming from the greenhouse gases, thereby providing the direct link to a mass extinction. Lastly, LIP emplacement occurred as multiple individual eruptions/intrusions with durations on timescales <100 ky over an extended time interval (<2 My). Associated degassing events would be much less buffered by the short- and long-term operating of the carbon cycle (e.g., weathering, ocean uptake of CO_2, and carbonate dissolution), therefore having the potential to be much more destructive to the climate and environment (see also McKenzie and Jiang 2019 this issue).

The best resolved feature of the $\delta^{13}C$ record of the Tr–J boundary beds is the short-lived (<100 ky) initial CIE (Fig. 5), a feature that clearly differs from the long-term P–Tr $\delta^{13}C$ trend. The magnitude of the excursion, as recorded in land plants, is extraordinary (up to 8‰) and requires the rapid release of huge volumes of ^{13}C-depleted carbon into the ocean and atmosphere. The eruption of the flood basalts of the Central Atlantic Magmatic Province (CAMP) was contemporary with (or slightly preceding) the initial CIE and, like the Siberian Traps, intrusion of sills into organic-rich strata may have added additional ^{13}C-depleted carbon into the system (Heimdal et al. 2018). However, such geologically brief negative CIEs are often attributed to the destabilization of methane hydrates (Dickens et al. 1995). Hydrates are ice-like deposits found at shallow depths in sediments beneath cold and/or deep waters. Methane hydrates are very ^{13}C-depleted ($\delta^{13}C \approx -60‰$), an effect of biological methane production and recycling during the anaerobic breakdown of organic matter. There are concerns today that modest increases in ocean temperature will cause methane hydrate deposits to destabilize and release large volumes of methane, a potent greenhouse gas, into the atmosphere and so further accelerate the warming trend. Such a positive Earth system feedback would appear as a geologically rapid event in the $\delta^{13}C$ record, such as the end-Triassic initial CIE. Methane hydrate destabilization has been proposed for the latest Triassic: it coincided closely with the mass extinction (Ruhl et al. 2011). However, it is puzzling that the emplacement of the CAMP and its thermogenic degassing over ~500 ky did not produce a protracted $\delta^{13}C$ trend like that seen during the P–Tr mass extinction.

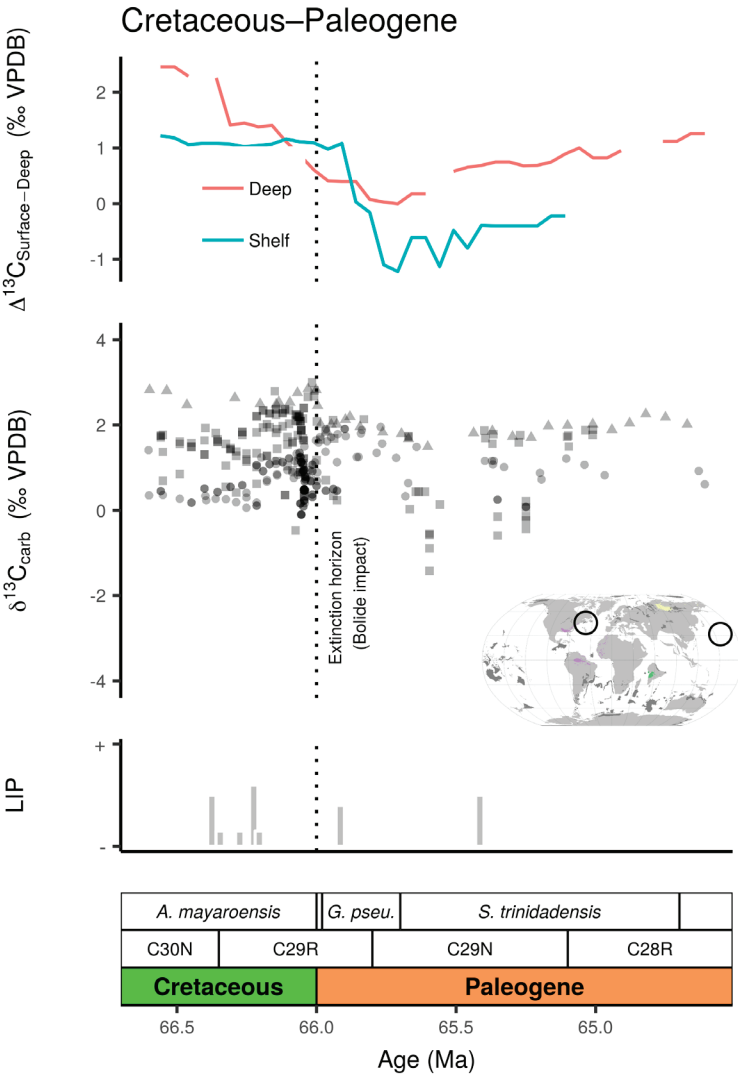

Figure 6 (**upper graph**) Trendlines for the surface-to-depth $\delta^{13}C$ gradient [given as $\Delta^{13}C_{Surface-Deep} = \delta^{13}C_{Surface} - \delta^{13}C_{Deep}$] for the deep ocean (red curve) and the continental shelf (blue curve) are constructed with a sliding window (span = 0.3 My) and using the data of the middle graph. (**middle graph**) Carbon isotope curve across the Cretaceous/Paleogene (K–Pg) boundary as taken from the Shatsky Rise (Ocean Drilling Program site 577; black circle on paleogeographic map, itself color coded as per Figure 1) and the New Jersey Shelf (East coast of America; black circle on paleogeographic map). Data from benthic samples (circles), planktic foraminifera (squares), and bulk fine fraction (triangles); Abbreviation: VPDB = Vienna Peedee belemnite. After Zachos et al. (1989) and Esmeray-Senlet et al. (2015). (**lower graph**) The LIP bar graph roughly represents the temporal evolution and intensity of volcanic Deccan Traps outpouring. On the timescale are marked the relevant magnetostratigraphic divisions [given in chrons (symbol 'C') and where N = normal polarity and R = reverse polarity] and biostratigraphic divisions [from oldest to youngest: *Abathomphalus mayaroensis*; *Globigerina eugubina*; *Globigerina pseudobulloides*; *Subbotina trinidadensis*]. After Zachos et al. (1989). The data is projected on a new timeline, based on new radiometric dates for the K–Pg boundary (Barnet et al. 2017 and references therein).

The convergence of planktic and benthic foraminfera shell $\delta^{13}C$ records at the K–Pg boundary has been a pivotal observation, which in the 1980s was considered as a signal of complete shutdown of primary productivity (e.g., Zachos et al. 1989) (Fig. 6). This scenario, termed a "Strangelove ocean", was considered to be consistent with the idea that a bolide impact caused the injection of dust and aerosol in the atmosphere and severely affected global photosynthetic activity (Alvarez et al. 1980). In today's oceans, DIC shows a carbon isotope gradient with values in surface waters being relatively enriched in ^{13}C than deeper waters, because ^{12}C is taken up by photosynthesizing plankton and incorporated into organic matter. Subsequent remineralization of the organic matter at depth returns the ^{13}C-depleted carbon to the DIC pool and drives the deep water $\delta^{13}C$ values to more negative values. In an ocean devoid of photosynthesizing plankton, this process does not happen and the surface-to-depth $\delta^{13}C$ gradient disappears. The Strangelove ocean hypothesis has now largely been dismissed. A modeling study has shown that a certain degree of organic carbon transport to the ocean floor ("export productivity") must have prevented the ocean's DIC carbon isotope composition to drift towards $\delta^{13}C$ values equal to the weathering flux (Kump 1991) (Fig. 3). Also, surviving bottom-dwelling fauna indicates that a food supply to the sea floor must have persisted (Alegret et al. 2012).

Other possible causes for the isotopic changes at the K–Pg boundary have been presented. One hypothesis is that the extinction saw a change in plankton composition to populations dominated by smaller species that, after death, were less likely to survive the descent to the sea floor (D'Hondt et al. 1998). In addition, the demise of zooplankton, which produce faecal pellets that facilitate export productivity, implies less ^{12}C-rich organic matter reaching the DIC pool at depth. If this process weakens, then most remineralization will occur near the surface and greatly diminish the surface-to-depth $\delta^{13}C$ gradient (D'Hondt et al. 1998). In another twist, Alegret et al. (2012) suggested that a community turnover among foraminifera species, and species-specific $\delta^{13}C$ signatures, could explain the disappearance of the surface-to-depth $\delta^{13}C$ gradient altogether. Finally, a purely physicochemical model has recently been proposed by Galbraith et al. (2015), which shows the effect of equilibration timescales on carbon isotope ratios via air–sea exchange, where high atmospheric CO_2 levels weakens the oceanic surface-to-depth $\delta^{13}C$ gradient. Clearly these are different scenarios to the original Strangelove ocean hypothesis, but the ideas share the notion that there were major changes in plankton populations and/or oceanographic conditions at the K–Pg boundary. There is also a close temporal association between the K–Pg extinction and volcanism, the Deccan Traps LIP (Figs. 2 and 6). Yet, intriguingly, these flood basalts seem to have had little effect on the carbon isotope record. The major difference of this LIP, with respect to the CAMP and the Siberian Traps, might be the lack of extensive intrusive magmatism into organic-rich sedimentary rock. On the other hand, volcanism could have already put ecosystems under stress prior to the Chicxulub (Mexico) bolide impact through volcanogenic CO_2 and SO_2 outgassing and consequent climatic changes. This may have contributed to the mass extinction (Barnet et al. 2017) (Fig. 6).

CONCLUSIONS

The carbon isotope records provide significant insights in the major environmental perturbations associated with mass extinctions, because they help quantify both magnitude and rates of change in the carbon cycle. Brief, high amplitude excursions, such as that seen during the Tr–J mass extinction, are the hallmark of rapid processes, such as the release of vast quantities of methane from hydrates. In contrast, the prolonged decline of $\delta^{13}C$ values during the P–Tr crisis points to longer-term processes, such as the cumulative effect of the release of thermogenic gases produced by baking of sediments beneath the Siberian Traps lava pile. The magnitude and duration of the P–Tr trends also eliminates other hypotheses, such as a catastrophic ocean overturn event. The rise of planktic foraminifera in the Jurassic means that, by the time of the

next mass extinction (at the end of the Cretaceous), it is possible to reconstruct the water column surface-to-depth $\delta^{13}C$ gradient. These data show there were major changes in plankton populations and/or oceanographic conditions during the K–Pg crisis.

Despite their versatility, carbon isotopes are not a panacea for understanding all aspects of mass extinctions. Most, perhaps all, extinction crises coincide with large-scale volcanism and disturbance to the long-term carbon cycle. But the associated carbon gas emissions might have left little imprint on $\delta^{13}C$ records. Additionally, failure to account for the limitations inherent to certain isotope recording mediums might lead to erroneous interpretations of carbon isotope excursions. Our evaluation further emphasizes the need for understanding global carbon reservoirs, fluxes, interconnections, and their respective carbon isotope compositions. Aspects such as timing, volumes, location of eruptions, and flux rates from LIP volcanism, likely to be important in extinction scenarios, can only be reliably addressed by including other proxy data, improved dating and computer modeling. As a result, there are several strands in the extinction–volcanism link that are poorly understood. This raises many questions. Why is the timeline of volcanic outpouring broad relative to the short duration of an extinction pulse? Why are some giant volcanic episodes that have an extensive intrusive component not associated with mass extinctions, such as the Paraná–Etendeka LIP or the North Atlantic Igneous Province, even though others are?

Looking forward, the release of greenhouse gasses by intrusive volcanism and through positive feedbacks (as for methane hydrates) provides a tantalizing clue in the search for the smoking gun of ancient extinction events. It also warns of the future effects of more recently emitted fossil carbon into the Earth system.

ACKNOWLEDGMENTS

We would like to thank Joost Frieling, Jacopo Dal Corso, Ulrich Struck and Henrik Svensen for insightful comments on earlier drafts, which significantly improved this work. We thank the Netherlands Earth and Life Sciences for grant NWO ALW 0.145 and the NERC Ecosystem Resilience and Recovery from the Permo-Triassic Crisis (EcoPT) for grant NE/P0137224/1.

REFERENCES

Alegret L, Thomas E, Lohmann KC (2012) End-Cretaceous marine mass extinction not caused by productivity collapse. Proceedings of the National Academy of Sciences of the United States of America 109: 728-732

Alvarez LW, Alvarez W, Asaro F, Michel HV (1980) Extraterrestrial cause for the Cretaceous-Tertiary extinction. Science 208: 1095-1108

Barnet JSK and 6 coauthors (2017) A new high-resolution chronology for the late Maastrichtian warming event: Establishing robust temporal links with the onset of Deccan volcanism. Geology 46: 147-150

Black BA, Gibson SA (2019) Deep carbon and the life cycle of large igneous provinces. Elements 15: 319-324

Burgess SD, Muirhead JD, Bowring SA (2017) Initial pulse of Siberian Traps sills as the trigger of the end-Permian mass extinction. Nature Communications 8, doi: 10.1038/s41467-017-00083-9

Cao C and 5 coauthors (2009) Biogeochemical evidence for euxinic oceans and ecological disturbance presaging the end-Permian mass extinction event. Earth and Planetary Science Letters 281:188-201

D'Hondt S, Donaghay P, Zachos JC, Luttenberg D, Lindinger M (1998) Organic carbon fluxes and ecological recovery from the Cretaceous-Tertiary mass extinction. Science 282: 276-279

Dickens GR, O'Neil JR, Rea DK, Owen RM (1995) Dissociation of oceanic methane hydrate as a cause of the carbon isotope excursion at the end of the Paleocene. Paleoceanography 10: 965-971

Esmeray-Senlet S and 5 coauthors (2015) Evidence for reduced export productivity following the Cretaceous/Paleogene mass extinction. Paleoceanography 30: 718-738

Galbraith ED, Kwon EY, Bianchi D, Hain MP, Sarmiento JL (2015) The impact of atmospheric pCO_2 on carbon isotope ratios of the atmosphere and ocean. Global Biogeochemical Cycles 29: 307-324

Hallam A, Wignall PB (1999) Mass extinctions and sea-level changes. Earth-Science Reviews 48: 217-250

Heimdal TH and 7 coauthors (2018) Large-scale sill emplacement in Brazil as a trigger for the end-Triassic crisis. Scientific Reports 8, doi: 10.1038/s41598-017-18629-8

Holser WT, Magaritz M (1987) Events near the Permian–Triassic boundary. Modern Geology 11: 155-180

Hotinski RM, Bice KL, Kump LR, Najjar RG, Arthur MA (2001) Ocean stagnation and end-Permian anoxia. Geology 29: 7-10

Johansson L, Zahirovic S, Müller RD (2018) The interplay between the eruption and weathering of large igneous provinces and the deep-time carbon cycle. Geophysical Research Letters: 5380-5389

Knoll AH, Bambach RK, Canfield DE, Grotzinger JP (1996) Comparative Earth history and Late Permian mass extinction. Science 273: 452-457

Knoll AH, Bambach RK, Payne JL, Pruss S, Fischer WW (2007) Paleophysiology and end-Permian mass extinction. Earth and Planetary Science Letters 256: 295-313

Kump LR (1991) Interpreting carbon-isotope excursions: Strangelove oceans. Geology 19: 299-302

Meyer KM, Kump LR, Ridgwell A (2008) Biogeochemical controls on photic-zone euxinia during the end-Permian mass extinction. Geology 36: 747-750

McKenzie NR, Jiang H (2019) The Earth's outgassing and climatic transitions: the slow-burn towards environmental "catastrophes"? Elements 15: 325-330

Rampino MR, Caldeira K (2005) Major perturbation of ocean chemistry and a 'Strangelove Ocean' after the end-Permian mass extinction. Terra Nova 17: 554-559

Raup DM, Sepkoski JJJr (1982) Mass extinctions in the marine fossil record. Science 215: 1501-1503

Ruhl M, Veld H, Kürschner WM (2010) Sedimentary organic matter characterization of the Triassic–Jurassic boundary GSSP at Kuhjoch (Austria). Earth and Planetary Science Letters 292: 17-26

Ruhl M, Bonis NR, Reichart G-J, Sinninghe Damsté JS, Kürschner WM (2011) Atmospheric carbon injection linked to end-Triassic mass extinction. Science 333: 430-434

Schobben M and 12 coauthors (2017) Latest Permian carbonate carbon isotope variability traces heterogeneous organic carbon accumulation and authigenic carbonate formation. Climate of the Past 13: 1635-1659

Svensen H and 6 coauthors (2009) Siberian gas venting and the end-Permian environmental crisis. Earth and Planetary Science Letters 277: 490-500

van de Schootbrugge B and 7 coauthors (2008) Carbon cycle perturbation and stabilization in the wake of the Triassic-Jurassic boundary mass-extinction event. Geochemistry, Geophysics, Geosystems 9, doi: 10.1029/2007GC001914

von Hillebrandt A and 12 coauthors (2013) The global stratotype sections and point (GSSP) for the base of the Jurassic System at Kuhjoch (Karwendel Mountains, Northern Calcareous Alps, Tyrol, Austria). Episodes 36: 162-198

Wignall PB (2015) The Worst of Times: How Life on Earth Survived Eighty Million Years of Extinctions. Princeton University Press, Princeton, 224 pp

Zachos JC, Arthur MA, Dean WE (1989) Geochemical evidence for suppression of pelagic marine productivity at the Cretaceous/Tertiary boundary. Nature 337: 61-64